ELSEVIER

Chemical Engineering Journal 86 (2002) 299–307

Chemical Engineering Journal

www.elsevier.com/locate/cej

Axial solid concentration distribution in tapered and cylindrical bubble columns

Kai Zhang*

Institute of Coal Chemistry, Chinese Academy of Sciences, P.O. Box 165, Taiyuan 030001, People's Republic of China

Received 20 March 2001; accepted 11 June 2001

Abstract

The distribution of axial solid concentration was investigated experimentally and theoretically in tapered and cylindrical slurry bubble columns using air as the gas phase, tap water as the liquid phase and quartz sands as the solid phase. Based on the sedimentation–dispersion model commonly used in cylindrical columns, a mathematical model was presented to predict the solid concentration distribution in the tapered column. Superficial gas velocities up to 0.28 m/s, slurry concentrations up to 159 kg(solid)/m^3(slurry), and static slurry height from 1.6 to 2.7 m were measured. The axial solid concentration distribution becomes uniform with an increase in superficial gas velocity or average solid concentration and with a decrease in particle diameter or static slurry height. The experiments were carried out in the cylindrical column under similar operating conditions to compare differences in the axial solid distribution measured in cylindrical and tapered columns. The results showed that the tapered column provides a more uniform profile of axial solid concentration than the cylindrical column. An empirical correlation for Peclet number was developed using dimensional analysis, which can predict the axial solid concentration distribution in tapered columns.

Keywords: Tapered slurry bubble column; Axial solid concentration distribution; Modified sedimentation–dispersion model

1. Introduction

Because of its good mixing characteristics, high heat and mass transfer rates, and fast chemical reaction, the slurry bubble column (SBC) has been widely employed in a variety of physical and chemical processes. These include dust collection, waste water treatment, and coal liquefaction [1,2]. Recently, the tapered slurry bubble column (TSBC) has received much attention in biochemical reaction [3] and waste water treatment [4]. One of the important features of TSBC is that the cross-sectional area is enlarged along the column height from the bottom to the top. At the bottom, the superficial gas velocity is relatively high to ensure suspension of large/heavy particles; at the top, it is relatively low to prevent entrainment of the small/light particles. Therefore, the tapered column can be operated over a wider range of particle size distribution than the conventional cylindrical column. The gas velocity decreases linearly from the bottom to the top in TSBC, so TSBC is more suitable than the cylindrical slurry bubble column (CSBC) to simulate the gas volumetric contraction reactions, such as Fischer–Tropsch synthesis and low-temperature liquid-phase methanol synthesis [5]. The majority of research concerning tapered columns has focused on gas–solid and liquid–solid systems, e.g. [6–8]. The literature in the area of gas–liquid–solid systems is mostly about CSBC [1,2]. The solid particles can be catalyst, reactant or product in a SBC. Quantitative analysis of the solid concentration profile in CSBC is based on the sedimentation–dispersion model [5,9–18], which is characterized by two parameters, i.e. the solid settling velocity and the axial solid dispersion coefficient. A number of empirical correlations have been proposed to predict these two parameters. However, the hydrodynamics in a TSBC has so far received relatively little attention.

In this work a one-dimensional sedimentation–dispersion model describing the axial solid concentration distribution in a TSBC is proposed. This model was verified with experimental data involving monodispersed and binary mixture of solid particles at different operating condition. The effect of superficial gas velocity, solid concentration, static slurry height, and particle diameter was all investigated. The method of Goossens et al. [19] was adopted to calculate the average diameter of binary mixtures. The synchronous sampling method was used to measure the axial solid concentration distribution. Similar experiments were carried out in

* Present address: Department of Chemical Engineering, University College London, Torrinston Place London WCIE 7JE, Pembroke Street, Cambridge CB2 3RA, UK. Tel.: +44-1223-344772; fax: +44-1223-334796.
E-mail address: zhangk98@yahoo.com (K. Zhang).

1385-8947/02/$ – see front matter
PII: S1385-8947(01)00190-5

Nomenclature

a, b, c, d, e	parameters in Eq. (12)
A, B	parameters in Eq. (7)
Ar	Archimedes number
C_B	solid concentration in the slurry at $x = h_B$, mass per volume (kg(solid)/m^3(slurry))
$\bar{C}_B$	dimensionless solid concentration in the slurry
C_s	solid concentration in the slurry, mass per volume (kg(solid)/m^3(slurry))
$\bar{C}_s$	dimensionless solid concentration in the slurry
C_p	average solid concentration in the slurry, mass per volume (kg(solid)/m^3(slurry))
C_{ps}	dimension average solid concentration in the slurry, mass per mass (kg(solid)/kg(slurry))
d_p	particle diameter (m)
$d_{p,m}$	average particle diameter of binary mixture (m)
D	column diameter at $x = h$ (see Fig. 3) (m)
D_B	column diameter at the base, i.e. at $x = h_B$ (see Fig. 3) (m)
E_{zs}	solid-phase axial dispersion coefficient (m^2/s)
Fr	Froude number
h	expand slurry height based on the conical base (see Fig. 3), $h = H + h_B$ (m)
h_B	distance from distributor to the conical base (m)
h_0	static slurry height based on the conical base (see Fig. 3), $h_0 = H_0 + h_B$ (m)
H	expand slurry height based on the distributor (see Fig. 3) (m)
H_0	static slurry height based on the distributor (see Fig. 3) (m)
m	weight percent of particle
n_s	mass flux of solid in the x-direction (kg/s m^2)
$\vec{n}_s$	mass flux of solid, a vector (kg/s m^2)
Pe	Peclet number
S_b	dimensionless area ratio (see Fig. 3)
t	time (s)
U_{st}	solid settling velocity (m/s)
x	axial coordinate based on the conical base, $x = X + h_B$ (m)
X	axial coordinate based on the distributor (m)
$\bar{X}$	dimensionless axial coordinate

Greek letters

μ_l	liquid viscosity (Pa m)
θ	taper angle (°)
ρ_l	liquid density (kg/m^3)
ρ_s	solid density (kg/m^3)
ρ_{sl}	slurry density (kg/m^3)

Operator

∇	divergence

the CSBC in order to understand the difference of axial solid concentration distribution between the TSBC and CSBC.

2. Experimental

Experimental data were collected in two different Plexiglas bubble columns, i.e. a tapered column and a cylindrical column. A schematic diagram of the experimental setup used in the present study is shown in Fig. 1. The axial solid distribution was measured by the synchronous sampling method. The TSBC can be divided into two sections: conical and cylindrical sections. The conical section was 3.00 m in height with an overall taper angle of 1.91°. Column size increased from 0.10 m i.d. at the bottom to 0.20 m i.d. at the top. The cylindrical section of 1.20 m height with diameter of 0.20 m was used to prevent slurry from overflowing. Eight sampling tubes were placed along the column at 0.05, 0.40, 0.80, 1.20, 1.60, 2.00, 2.40 and 2.80 m above the distributor, respectively. These were used to obtain solid samples. The CSBC was 0.10 m in internal diameter and 4.75 m in height. Eight sampling tubes were also placed along the column, but at 0.05, 0.20, 0.40, 0.80, 1.20, 1.60, 2.00 and 2.80 m above the distributor, respectively.

Although the sample withdrawal method has its own shortcomings [20], it remains a commonly used technique [5,9–18,21]. The sampling system used is shown in Fig. 2.

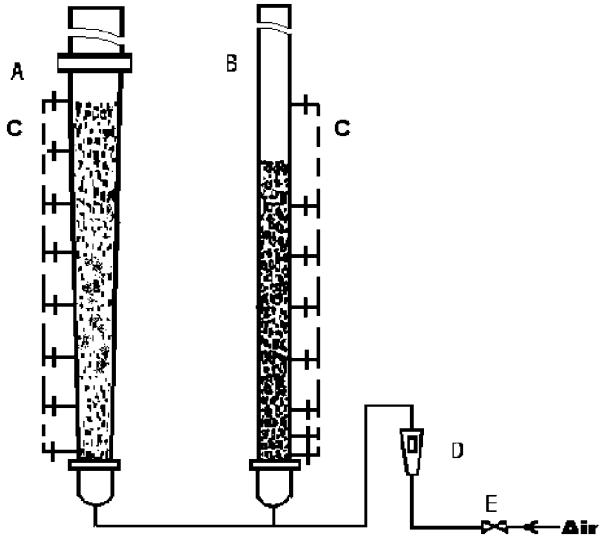

Fig. 1. Schematic diagram of the experimental setup: (A) TSBC; (B) CSBC; (C) sampling system; (D) rotameter; (E) valve.

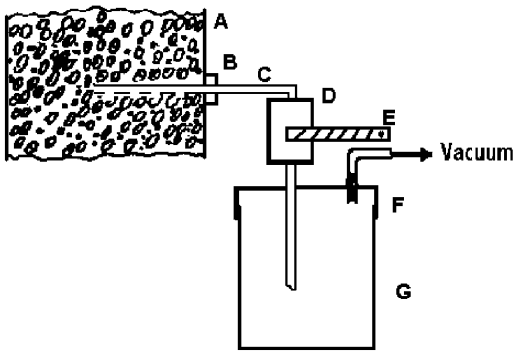

Fig. 2. Schematic diagram of the sampling apparatus: (A) column; (B) sample port; (C) sample tube; (D) globe valve; (E) handle; (F) tank cover; (G) sample tank.

The Plexiglas sample tank of 80 mm high and 32 mm internal diameter was used. The stainless steel sample tube was 6 mm in internal diameter with a wall thickness of 1 mm. Four holes (5 mm i.d.) were positioned facing vertically downwards in each pipe to allow the sampling of slurry (to be collected into the tank) at different radial locations at the desired axial position. It was necessary to withdraw the samples simultaneously from the various axial ports. This was achieved by using synchronous ball valves and withdrawing the samples under vacuum, thus allowing the slurry sample to enter the sample tank quickly through the tube. To investigate the potential effect of particle inertia, a preliminary experiment was carried out in a mechanically stirred tank to optimize the sampling tube design and to select suitable vacuum condition for the liquid–solid systems used [5]. It was also used to test the reliability of the sample withdrawal method by comparing the total amount of solids calculated from the solid concentration profile with the initial amount added to the column for each run.

All experiments were carried out at atmospheric pressure and a room temperature of approximate 25 °C. The three-phase system was composed of air, tap water and quartz sand. The gas flow was continuous whilst the slurry was batchwise. Four types of quartz sands were used as the monodispersed particles. The physical properties of the liquid and solid are listed in Table 1. For experiments involving

Table 1
The physical properties of the liquid and solid

Tap water	
Density (kg/m^3)	997
Viscosity (Pa s)	1
Quartz sand	
Diameter 1 (D_1) (m)	70.0 (50.0–90.0) $\times$ 10^{-6}
Diameter 2 (D_2) (m)	107.5 (90.0–125.0) $\times$ 10^{-6}
Diameter 3 (D_3) (m)	142.5 (125.0–160.0) $\times$ 10^{-6}
Diameter 4 (D_4) (m)	180.0 (160.0–200.0) $\times$ 10^{-6}
Binary mixture (Mix)	D_2 and D_4
Density (kg/m^3)	2636

Table 2
Experimental conditions

Operating condition	Range
Superficial gas velocity (m/s)	0.02–0.28
Average slurry concentration (kg(solid)/m^3(slurry))	53–159
Average particle diameter	D_1, D_2, D_3, D_4, Mix
Static slurry height (m)	1.60–2.40
Distributor	
Type	Perforated plate
Orifice diameter (m)	8×10^{-4}
Open area (%)	0.4

a binary mixture of particles, the average diameter of binary mixtures was calculated using the definition of Goossens et al. [19]:

$$d_{p,m} = \frac{d_{p,1}d_{p,2}}{m_1 d_{p,2} + m_2 d_{p,1}} \quad (1)$$

where d_p is particle diameter and m is the weight percent of the particles. Subscripts 1 and 2 represent different compositions in the binary system. It should be noted that the superficial gas velocity in a tapered slurry bubble column is based on the bottom cross-sectional area so as to compare with the results in the CSBC. The operating conditions are summarized in Table 2.

In each experiment, the desired amount of tap water and quartz sand was first fed into the column. The air from the compressor was measured by a rotameter and then introduced into the column through gas distributor located at the bottom of the column. After steady state was established, samples were withdrawn as described below:

1. To turn on the vacuum connecting the sampling system.
2. To open the ball valves between the column and the sample tanks at the same time.
3. To turn off the vacuum when the slurry occupies the 2/3 of the sample tank, i.e. the volume of sample was about 43 cm^3.
4. To determine the solid concentration of slurry by using a gravimetrical method, i.e. weighting of slurry, preliminary separation of solid from water, drying and weighting of solid. The individual weights of the binary mixtures can be obtained by using a sieving method. More details of the experimental setup and procedures can be found in Zhang [5].

3. Modified sedimentation–dispersion model

Quantitative description of the axial sold concentration distribution in CSBC has been mainly based on the so-called sedimentation–dispersion model, originally proposed by Cova [9] and Suganuma and Yamanishi [10]. In this model, the concept of the widely used axial dispersion model was applied to the slurry phase, which was treated

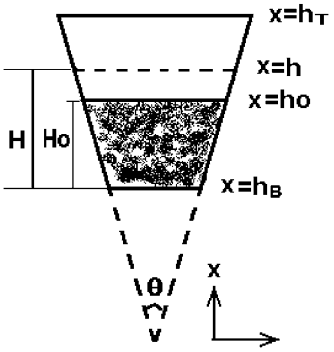

Fig. 3. Schematic diagram of the tapered column.

as a pseudo-homogeneous phase. A solid axial "dispersion" flux and a solid "sedimentation" flux superimposed on the overage slurry convection flux are considered, and thus it is termed the "sedimentation–dispersion" model.

As shown in Fig. 3, the continuity equation for solid phase for a differential element is

$$\frac{\partial C_s}{\partial t} + \nabla \cdot \vec{n}_s = 0 \tag{2}$$

With the assumption there are no radial gradients, Eq. (2) leads to the following equation:

$$\frac{\partial C_s}{\partial t} + \frac{\partial n_s}{\partial x} = 0 \tag{3}$$

The mass flux, n_s, is represented by a modification of Fick's law. The resultant equation is

$$n_s = C_s U_{st} + E_{zs} \frac{\partial C_s}{\partial x} \tag{4}$$

The first term on the right-hand side of Eq. (4) represents the net motion of solid particles due to the difference between sedimentation and convection fluxes, characterized by the solid settling velocity, U_{st}. The second term on the right-hand side of Eq. (4) is the dispersive transport, which is assumed to obey Fick's law, and is characterized by the solid dispersion coefficient, E_{zs}.

Substituting Eq. (4) into Eq. (3), we have

$$\frac{\partial C_s}{\partial t} + U_{st} \frac{\partial C_s}{\partial x} + E_{zs} \frac{\partial^2 C_s}{\partial x^2} = 0 \tag{5}$$

For steady state, $\partial C_s / \partial t = 0$. Thus,

$$U_{st} \frac{\partial C_s}{\partial x} + E_{zs} \frac{\partial^2 C_s}{\partial x^2} = 0 \tag{6}$$

The general solution of Eq. (6) can be expressed as

$$C_s = A + B \exp\left(-\frac{U_{st}}{E_{zs}} x\right) \tag{7}$$

where constants A and B depend on the boundary conditions chosen. Two different sets of boundary conditions for the slurry–batch system are as follows:

at the bottom of the colum ($x = h_B$),	$C_s = C_B$
when $x \to \infty$,	$C_s \to 0$

The solution of Eq. (7) is given as

$$C_s = \frac{C_B}{\exp((-U_{st}/E_{zs}) h_B)} \exp\left(-\frac{U_{st}}{E_{zs}} x\right) \tag{8}$$

Substituting $x = X + h_B$ in Eq. (8) and simplifying it, we have

$$C_s = C_B \exp\left(-\frac{U_{st}}{E_{zs}} X\right) \tag{9}$$

There are various correlations in the literature, e.g. [11,12] for estimating solid settling velocity, U_{st}. As shown in Eq. (9), U_{st}/E_{zs} and C_B can be obtained by regression analysis of solid concentration versus axial position data. However, if we want to obtain one parameter of U_{st} and E_{zs}, the other one must be assumed. Thus, U_{st} and E_{zs} are not separable for Eq. (9).

We define dimensionless variables as follows:

$$\bar{X} = \frac{X}{H}, \qquad \bar{C}_s = \frac{C_s}{C_p}, \qquad \bar{C}_B = \frac{C_B}{C_p}, \qquad Pe = \frac{U_{st} H}{E_{zs}}$$

We can rearrange Eq. (9) to

$$\bar{C}_s = \bar{C}_B \exp(-Pe\, \bar{X}) \tag{10}$$

4. Results and discussion

Axial solid concentration distributions were measured as described in Section 2. The experiments were conducted three times under the same operating conditions and the average value was regarded as the solid concentration. The amount of solid, calculated by Eq. (10), was found to be in good agreement with the initial amount added to the column for each run. The relative error is less than 5.5%.

4.1. Effect of particle diameter

The experimental solid distributions for different sizes of quartz sand are presented in Figs. 4–6. For monodispersed particles, the smaller the particle size, the more uniform the axial solid concentration distribution is found to be. This can be explained by a decrease in the solid settling velocity (U_{st}) with decreasing particle size. Many researchers [5,9–18] reached the same conclusion in CSBC. For the binary mixtures results presented in Fig. 6, the concentration of larger particles are higher than that of smaller particles at the bottom, while the concentration of smaller particles are higher than that of larger particles at the top. This is consistent with CSBC results [5,14].

4.2. Effect of superficial gas velocity

Fig. 7 illustrates the effect of superficial gas velocity on the axial solid concentration. An increase in superficial gas velocity leads to a more uniform concentration distribution. Turi and Ng [13], Bukur et al. [18] and Zhang [5]

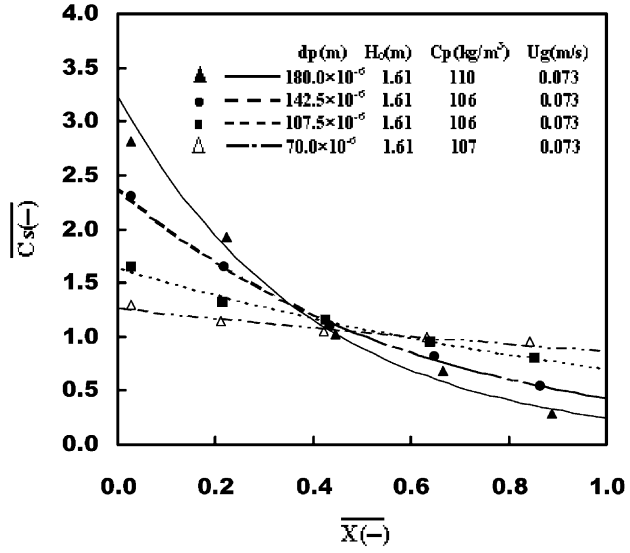

Fig. 4. Effect of particle diameter on axial solid concentration profile at $U_g = 0.073$ m/s.

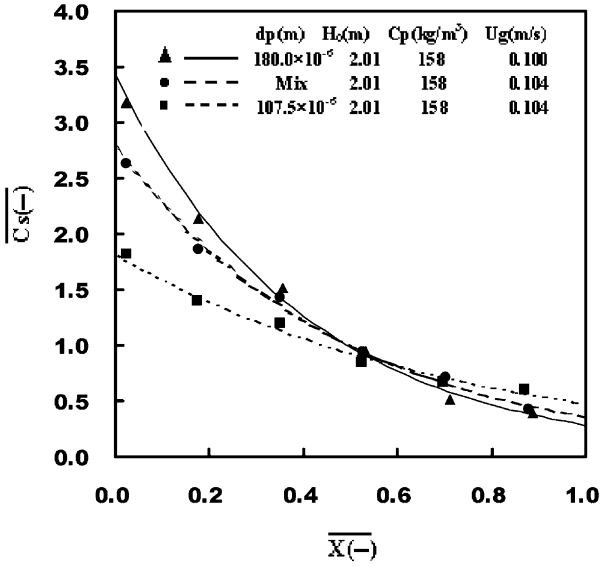

Fig. 6. Comparison of axial solid concentration distribution for monodispersed and binary particles.

came to the same conclusion in CSBC. This results from an increase in the solid dispersion coefficient (E_{zs}) with increasing superficial gas velocity. Drag coefficient increases with an increase of superficial gas velocity, which results in a decrease of solid settling velocity (U_{st}). It is clear that not all solid particles are suspended in the slurry when the gas velocity is 0.02 m/s.

4.3. Effect of slurry concentration

Figs. 8 and 9 illustrate results from experiments conducted with slurries containing different concentration of 180×10^{-6} and 107.5×10^{-6} m sands. These results show that axial solid concentration profile becomes uniform with increasing average slurry concentration. The most plausible explanation is that increasing solid concentration increases the "pseudo-viscosity" of the slurry, which in turn increases the drag coefficient and then decreases solid settling velocity (U_{st}). This results in a uniform profile of axial solid concentration. This kind of phenomenon also exists in CSBC [5].

4.4. Effect of static slurry height

The influence of the dimensionless static slurry height on axial solid concentration is too slight to be considered when its length is between 1.5 and 2.5 m in CSBC [5]. However,

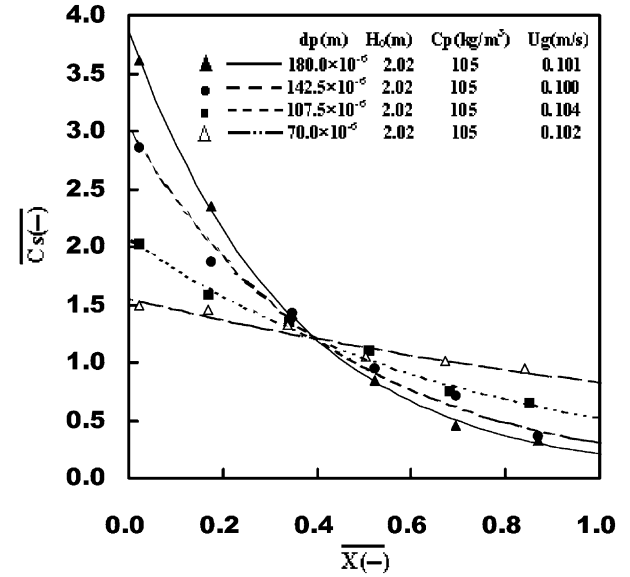

Fig. 5. Effect of particle diameter on axial solid concentration profile at $U_g = 0.10$ m/s.

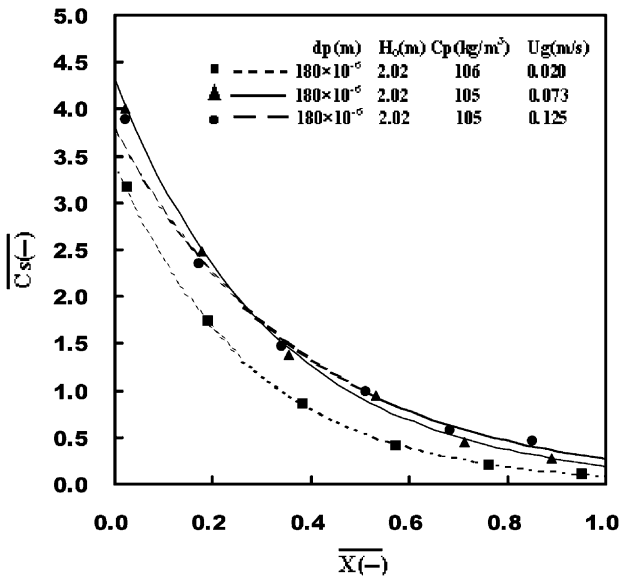

Fig. 7. Effect of superficial gas velocity on axial solid concentration distribution.

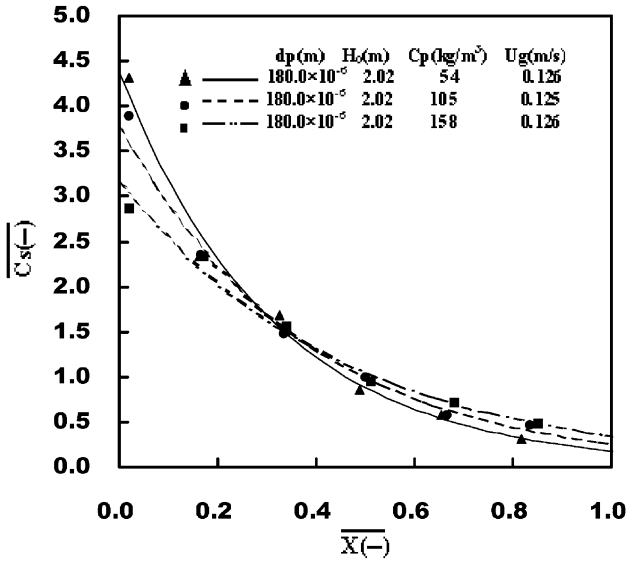

Fig. 8. Effect of average slurry concentration on axial solid concentration distribution for 180×10^{-6} m sand.

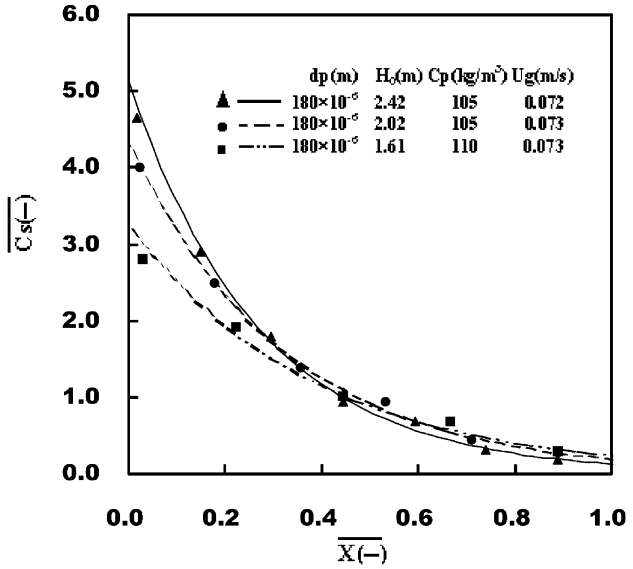

Fig. 10. Effect of static slurry height on axial solid concentration distribution for 180×10^{-6} m sand.

the gradient of axial solid concentration profile becomes steep when static slurry becomes high in TSBC as shown in Figs. 10 and 11. The most probable reason is that the superficial gas velocity decreases from the bottom to the top in TSBC.

4.5. Comparison of axial solid concentration distributions in TSBC and CSBC

Figs. 12–14 compare axial solid concentration distributions for 180×10^{-6}, 142.5×10^{-6} and 107.5×10^{-6} m sands in a TSBC and CSBC under similar operating conditions.

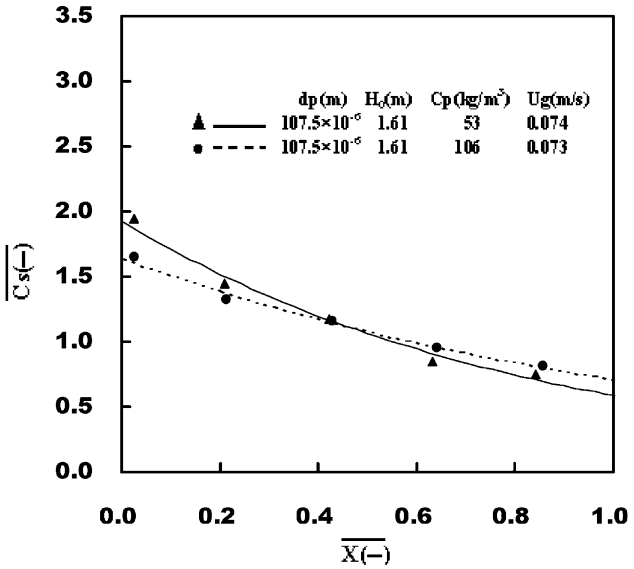

Fig. 9. Effect of average slurry concentration on axial solid concentration distribution for 107.5×10^{-6} m sand.

As mentioned above, the superficial gas velocity in a TSBC is based on the cross-sectional area of the bottom of the column. It is clear that a TSBC provides more uniform profile of axial solid concentration than a CSBC. Therefore, the actual axial solid concentration distribution is more uniform than the simulated data obtained from the conventional cylindrical column for the gas volumetric contraction reaction. The main features of TSBC are as follows:

1. It is convenient for solids with a wide particle size distribution, which can ensure the suspension of large/heavy

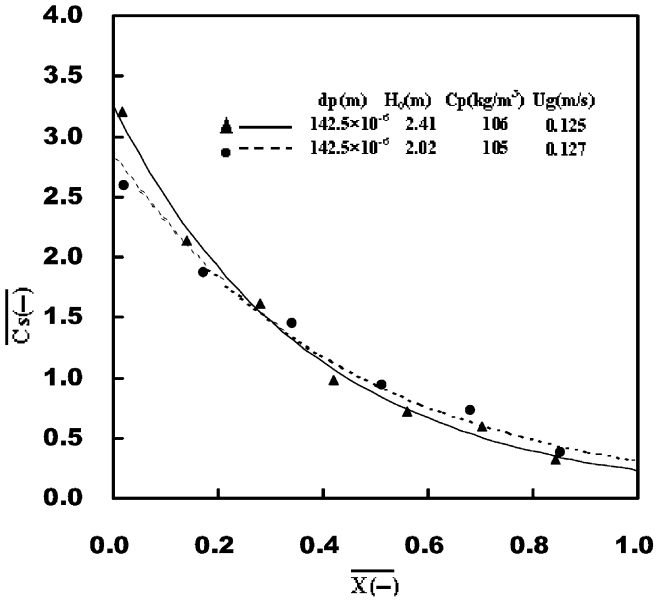

Fig. 11. Effect of static slurry height on axial solid concentration distribution for 142.5×10^{-6} m.

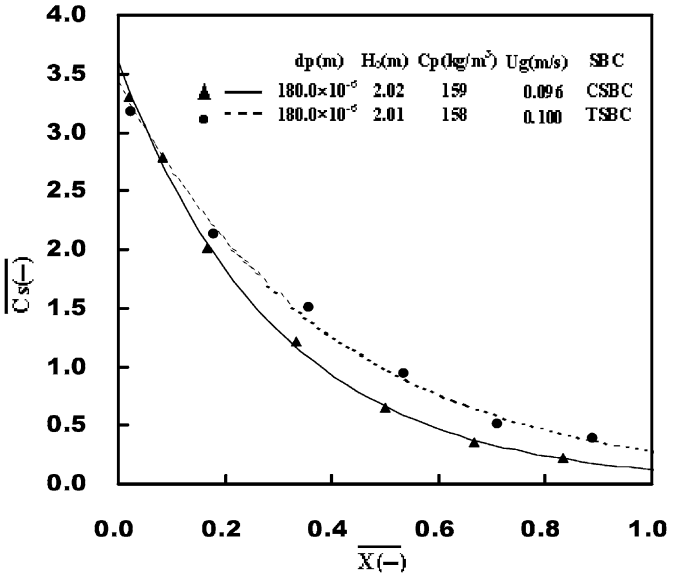

Fig. 12. Comparison of axial solid concentration distribution in TSBC and CSBC for 180×10^{-6} m sand.

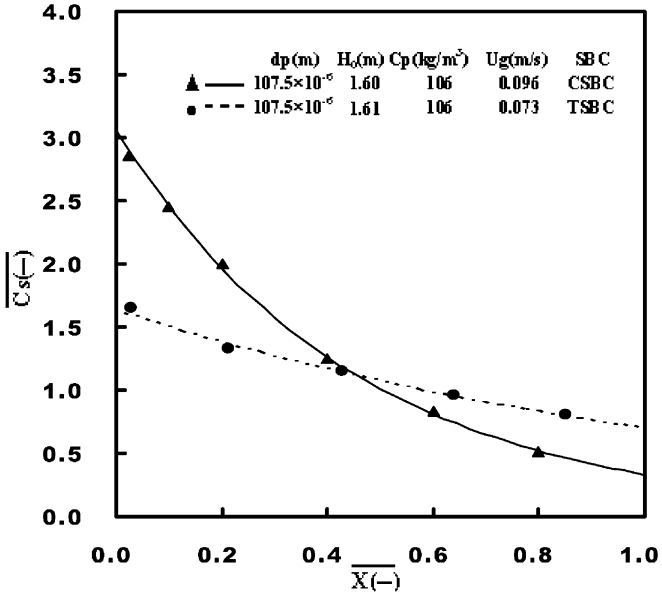

Fig. 14. Comparison of axial solid concentration distribution in TSBC and CSBC for 107.5×10^{-6} m sand.

particles, since gas velocity is relatively high at the bottom, and prevent entrainment of the small/light particles since gas velocity is relatively low at the top.

2. It is easier to control operating temperature with a TSBC than a CSBC for strong exothermal reactions, such as Fischer–Tropsch synthesis and liquid-phase methanol synthesis.

4.6. Correlation for the Peclet number

A small Peclet number indicates that the particle dispersion forces overcome the particle settling forces. This gives a small exponential coefficient in Eq. (10) and results in a homogeneous state of suspension. An inhomogeneous state of suspension corresponds to high Peclet number, resulting in a curved axial solid concentration distribution with the highest concentration at the column base. Some researchers [11,12] provided empirical correlations for the prediction of Peclet number. However, all the correlations available in the literature were correspond to the cylindrical column. Dimensionless analysis is used here to relate the Peclet number to the relevant physical parameters, including the apparatus size. Solid concentration profile in a slurry bubble column is a result of the balance of buoyancy, gravitational and drag forces. Therefore, Peclet number can be expected to be a function of the following eight parameters:

$$Pe = F(U_g, C_p, d_p, D, D_B, \rho_l, \rho_s, \mu_l) \quad (11)$$

where U_g, C_p, d_p, ρ and μ are superficial gas velocity based on the bottom cross-section area, average solid concentration, particle diameter, column diameter, density and viscosity, respectively. D_B is the column diameter at base and D is the column diameter at $x = H$. Dimensionless analysis suggests the Peclet number be a function of the following dimensionless groups:

$$Pe = a\,Fr^b\,Ar^c(1 - C_{ps})^d S_b^e \quad (12)$$

where the Froude number is defined as

$$Fr = \frac{U_g}{\sqrt{gD_B}} \quad (13)$$

and the Archimedes number is

$$Ar = \frac{d_p^3 g(\rho_s - \rho_l)\rho_l}{\mu_l^2} \quad (14)$$

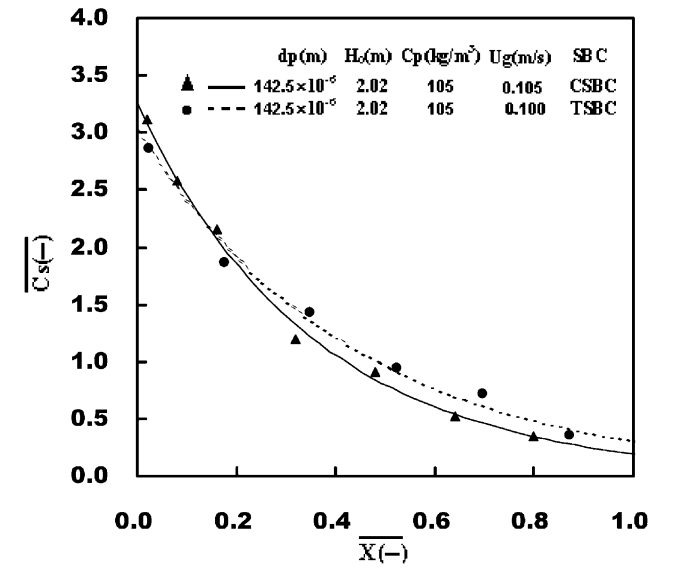

Fig. 13. Comparison of axial solid concentration distribution in TSBC and CSBC for 142.5×10^{-6} m sand.

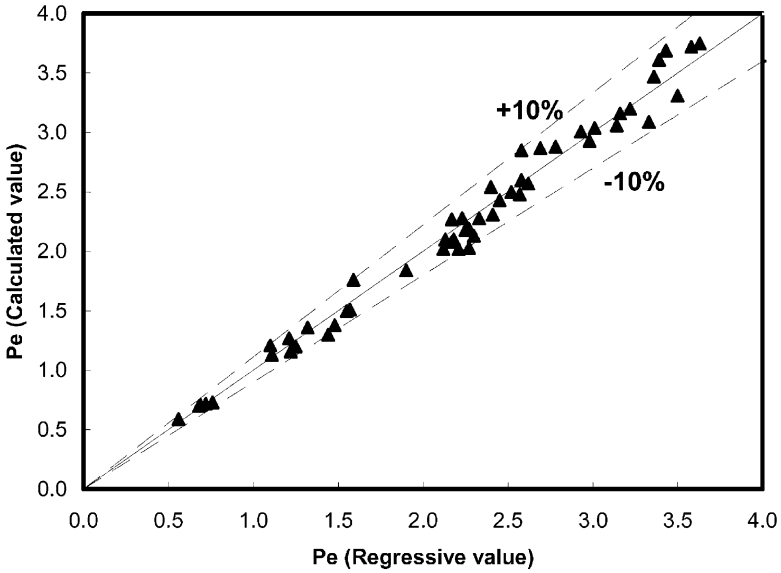

Fig. 15. Comparison of regressive and calculated Peclet numbers.

The dimensionless average concentration, C_{ps}, is defined as

$$C_{ps} = \frac{C_p}{\rho_{sl}} \tag{15}$$

and the ratio of area (see Fig. 3), S_b, is

$$S_b = \frac{D^2}{D_B^2} = \frac{h^2}{h_B^2} \tag{16}$$

where S_b is the influence of taper angle and static slurry height.

By applying the least-squares method to these data, the following correlation for Peclet number in TSBC is obtained as follows:

$$Pe = 0.0814 Fr^{-0.0526} Ar^{0.509} \left(1 - \frac{C_s}{\rho_{sl}}\right)^{0.954} S_b^{1.256} \tag{17}$$

Comparisons of regressive and calculated Peclet number are plotted in Fig. 15. The calculated Peclet numbers agree with the experimental Peclet numbers with a maximum deviation of 12% and an average standard deviation of 4.5% for both monodispersed particles and binary mixtures.

5. Conclusion

The axial solid concentration distribution in a tapered slurry bubble column was investigated using a synchronous sampling technique under different operating conditions. The axial distribution of solid concentration was found to become more uniform with increasing superficial gas velocity or slurry concentration and decreasing particle diameter or static slurry height. A TSBC can provide more uniform profile of axial solid concentration than a CSBC.

The reason that axial solid concentration profile becomes uniform with decreasing diameter is that solid settling velocity decreases with decreasing particle size. Furthermore, the larger particles concentrate at the bottom, whilst the smaller particles concentrate at the top for binary mixture. The solid dispersion coefficient increases with increasing superficial gas velocity or average slurry concentration, which leads to a more uniform profile of axial solid concentration. The effect of static slurry height on the axial solid concentration profile is attributed to the decrease in superficial gas velocity from the bottom to the top in a TSBC.

Based on the balance of solids suspended in the slurry, a dimensionless empirical correlation for Peclet number was proposed. The calculated Peclet number appears in good agreement with the experimental regressive Peclet number.

Acknowledgements

This research was funded by National Natural Science Foundation of China (NNSFC) and Royal Society of London. I would like to thank Professors Bijiang Zhang and Yulong Zhao for their valuable guidance. I would also like to acknowledge the kind hospitality of Professor Rex Thorpe and the Department of Chemical Engineering whilst I spent at University of Cambridge as a Royal Society Royal Fellow.

References

[1] L.S. Fan, Gas–Liquid–Solid Fluidization Engineering, Butterworths, Stoneham, MA, 1989.
[2] M.P. Dudukovic, F. Larachi, P.L. Mills, Multiphase reactors—revisited, Chem. Eng. Sci. 54 (13/14) (1999) 1975–1995.
[3] J.S. Huang, J.L. Yan, C.S. Wu, Comparative bioparticle and hydrodynamic characteristics of conventional and tapered anaerobic

fluidized-bed bioreactors, J. Chem. Tech. Biotech. 75 (4) (2000) 269–278.
[4] D.D. Lee, C.D. Scot, C.W. Hancher, Fluidized-bed bioreactor for coal-conversion effluents, J. WPCF 51 (5) (1979) 974–984.
[5] K. Zhang, Investigation on fluid dynamics in bubble slurry columns, M.Eng. Thesis, Institute of Coal Chemistry, Chinese Academy of Sciences, 1992 (in Chinese).
[6] Y.F. Shi, Y.S. Yu, L.T. Fan, Incipient fluidization for a tapered fluidized bed, I&EC Fundam. 23 (4) (1984) 484–489.
[7] T. Maruyama, H. Sato, Liquid fluidization in conical vessels, Chem. Eng. J. 46 (1991) 15–21.
[8] G.H. Webster, J.J. Perona, Liquid mixing in a tapered fluidized bed, AIChE J. 34 (8) (1988) 1398–1402.
[9] D.R. Cova, Catalyst suspension in gas-agitated tubular reactors, I&EC Process Des. Dev. 5 (1) (1966) 20–32.
[10] T. Suganuma, T. Yamanishi, Behaviors of solid particles in gas bubble columns, Kagaku Kogaku 30 (1966) 1136–1140.
[11] K. Kato, A. Nishiwaki, T. Fukuda, S. Tanaka, The behavior of suspended solid particles and liquid in bubble columns, J. Chem. Eng. Jpn. 5 (1972) 112–118.
[12] D.N. Smith, J.A. Ruether, Dispersed solid dynamics in a slurry bubble column, Chem. Eng. Sci. 40 (50) (1985) 741–754.
[13] E. Turi, K.M. Ng, Axial distribution of solid particle in bubble column slurry reactors in the bubble flow regime, Chem. Eng. Commun. 46 (1986) 323–345.
[14] M.N. Badgujar, A. Deimling, B.I. Morsi, Y.T. Shah, N.L. Carr, Solids distribution in a batch bubble column, Chem. Eng. Commun. 48 (1986) 127–153.
[15] D.N. Smith, J.A. Ruether, Y.T. Shah, M.N. Badgujar, Modified sedimentation–dispersion model for solids in a three-phase slurry column, AIChE J. 32 (3) (1986) 426–436.
[16] W. O'Dowd, D.N. Smith, J.A. Ruether, S.C. Saxena, Gas and solids behavior in a baffled and unbaffled slurry bubble column, AIChE J. 33 (12) (1987) 1959–1970.
[17] I.G. Reilly, D.S. Scott, T.J.W. De Bruijn, D. MacIntyre, J. Piskorz, Axial solids concentrations in three-phase bubble column, Chem. Eng. Sci. 45 (8) (1990) 2293–2299.
[18] D.B. Bukur, A.S. Patel, J.G. Daly, Gas holdup and solids dispersion in a three-phase slurry bubble column, AIChE J. 36 (11) (1990) 1731–1735.
[19] W.R.A. Goossens, G.L. Dumont, G.L. Spaepen, Fluidization of binary mixtures in the laminar flow region, Chem. Eng. Prog. Symp. Ser. 67 (1971) 38–45.
[20] R.S. MacTaggart, H.A. Nasr-El-Din, J.H. Masliyah, Sample withdrawal from a slurry mixing tank, Chem. Eng. Sci. 48 (5) (1993) 921–931.
[21] N. Dohi, Y. Matsuda, N. Itano, K. Minelkawa, T. Takahashi, Y. Kawase, Suspension of solid particles in multi-impeller three-phase stirred tank reactors, Can. J. Chem. Eng. 79 (1) (2001) 107–111.